<div style="text-align:center">

Supporting Information for

</div>

Activating Dual Atomic Electrocatalysts for Nitric Oxide Reduction Reaction through P/S Element

Yanmei Zang, Qian Wu[*], Shuhua Wang, Baibiao Huang, Ying Dai[*] and Yandong Ma[*]

School of Physics, State Key Laboratory of Crystal Materials, Shandong University, Shandanan Street 27, Jinan 250100, China

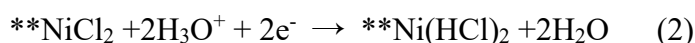*Email: wuq@mail.sdu.edu.cn (Q.W.); daiy60@sina.com (Y.D.); yandong.ma@sdu.edu.cn (Y.M.)

Note 1: Discussion on the substrate

We test graphene as substrate to anchor P/S and TM atoms (P/S−TM@NC). However, the formation energies of these candidate systems are all positive (**Table S1**), indicating their poor stability. Considering CN-supported single and dual atomic catalysts have attracted increasing interest recently [1-3], we select monolayer CN as the substrate.

The formation energies on P/S−TM@NC are calculated following $\Delta E_{form} = E_{P/S−TM@NC} + 8*\mu_C − (E_{graphene} + 6*\mu_N + \mu_{P/S} + \mu_{TM})$, where $E_{P/S−TM@NC}$, $E_{graphene}$, $\mu_C, \mu_N, \mu_{P/S}$ and μ_{TM} refer to the total energies of P/S−TM@NC, pristine graphene, and the chemical potential of C, N, P/S and TM atoms, respectively.

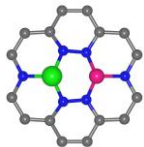**Note 2:** The synthesizability of the S−TM@CN

Recently, S-doped C_2N has been fabricated with the facile two-step template-free strategy [4], and we note that the formation energies of P/S-doped CN are more negative than that of the experimentally synthesized P/S-doped C_2N [5]. The P/S-doped CN can be obtained following the method of S-doped C_2N. Then P/S−TM@CN are obtained by further introducing TM atom on P/S-doped CN. Here, we use S−Ni@CN as an example to elucidate the experimental feasibility. Inspired by previous work [6,7], we choose $NiCl_2$ as the metal precursor, and synthetic route are shown as follow (**Fig. S5**):

$$NiCl_2 + ** \rightarrow **NiCl_2 \qquad\qquad (1)$$

$$**NiCl_2 + 2H_3O^+ + 2e^- \rightarrow **Ni(HCl)_2 + 2H_2O \qquad (2)$$
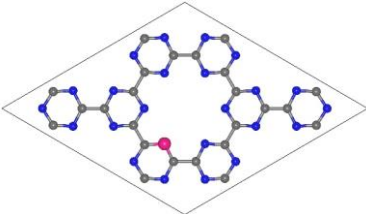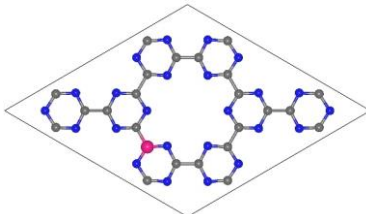
$$**Ni(HCl)_2 \rightarrow **Ni + 2HCl \qquad\qquad (3)$$

where ** refers to S-doped CN.

The results show that step (1) and step (2) are the spontaneous process without energy input. And for the last step, HCl is removed from S−Ni@CN with the energy barrier of 0.45 eV. Such small energy barrier can be overcome at room temperature, thus S−Ni@CN is expected to be synthesized in the experiment.

Table S1. The calculated formation energies for P/S−TM@NC

Catalysts	ΔE_{form} (eV)	Catalysts	ΔE_{form} (eV)
Configuration			
P−Ti@NC	5.11	S−Ti@NC	6.03
P−V@NC	5.79	S−V@NC	6.14
P−Cr@NC	11.12	S−Cr@NC	6.38
P−Mn@NC	5.28	S−Mn@NC	5.27
P−Fe@NC	6.09	S−Fe@NC	4.79
P−Co@NC	5.72	S−Co@NC	5.32
P−Ni@NC	5.57	S−Ni@NC	6.28
P−Cu@NC	6.32	S−Cu@NC	10.91

Table S2. The calculated formation energies for P/S-doped CN via N- and C-sites.

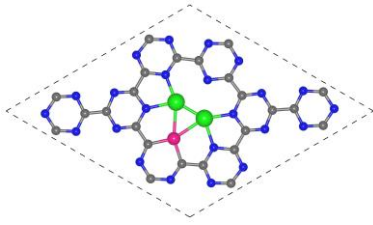| Catalysts	$E_{form(N)}$ (eV)	$E_{form(C)}$ (eV)
Configuration		

P-CN	0.86	1.80
S-CN	0.20	3.18

Table S3. The calculated binding energies (E_b), formation energies (E_f) and dissolution potential of metals (U_{diss}) for Type1 configuration of P/S−TM@CN. And the standard dissolution potential (U°_{diss}) of metal atoms and number of transferred electrons (N_e) during the dissolution.
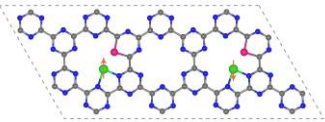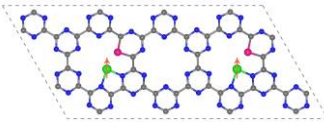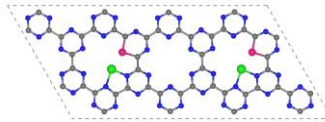
Catalysts	E_b	E_f	U_{diss}	U°_{diss}	N_e
P–Ti@CN	-1.77	-3.67	0.20	-1.63	2
P–V@CN	-0.79	-2.69	0.16	-1.18	2
P–Cr@CN	-0.76	-2.66	0.42	-0.91	2
P–Mn@CN	-1.32	-3.22	0.42	-1.19	2
P–Fe@CN	-0.03	-1.92	0.51	-0.45	2
P–Co@CN	-0.14	-2.04	0.74	-0.28	2
P–Ni@CN	-0.31	-2.20	0.84	-0.26	2
P–Cu@CN	-0.34	-2.24	1.46	0.34	2
S–Ti@CN	-1.49	- 4.05	0.39	-1.63	2
S–V@CN	-0.62	-3.17	0.41	-1.18	2
S–Cr@CN	-0.54	-3.09	0.64	-0.91	2
S–Mn@CN	-1.33	-3.88	0.75	-1.19	2
S–Fe@CN	0.37	-2.18	0.64	-0.45	2
S–Co@CN	0.29	-2.26	0.85	-0.28	2
S–Ni@CN	-0.15	-2.70	1.09	-0.26	2
S-Cu@CN	-0.18	-2.73	1.71	0.34	2

Table S4. The calculated binding energies for P/S−2TM@CN.

Catalysts	$E_{binding}$ (eV)	Catalysts	$E_{binding}$ (eV)

Configuration			
P–2Ti@CN	0.77	S–2Ti@CN	1.23
P–2V@CN	0.22	S–2V@CN	0.67
P–2Cr@CN	0.99	S–2Cr@CN	1.47
P–2Mn@CN	-0.06	S–2Mn@CN	0.81
P–2Fe@CN	0.65	S–2Fe@CN	–
P–2Co@CN	0.33	S–2Co@CN	–
P–2Ni@CN	-0.26	S–2Ni@CN	0.70
P–2Cu@CN	-0.13	S–2Cu@CN	0.71

Table S5. The total energies of different magnetic configurations for P–Cu@CN and S–Cu@CN with and without consideration of the Hubbard U correlation effect.

Catalysts	AFM (eV)	FM (eV)	NM (eV)
P-Cu@CN (without U)	–	–	-816.21
P-Cu@CN (with U)	–	–	-813.85
S-Ni@CN (without U)	-817.85	-817.85	-817.30
S-Ni@CN (with U)	-814.87	-814.87	-813.60

Table S6. The magnetic moment of TM for P–Cu@CN and S–Ni@CN with and without consideration of the Hubbard U correlation effect.

Catalysts	Magnetic moment (without U) (μ_B)	Magnetic moment (with U) (μ_B)
P–Cu@CN	0.00	0.00
S–Ni@CN	0.84	0.93

Table S7. Comparison of adsorption energy of *NO and *N_2 with and without H atom adsorption on P–Ti/P–V/P–Cr/P–Mn/P–Co/P–Ni/P–Cu@CN.

	*NO (without H atom) (eV)	*NO (with H atom) (eV)	*N_2 (without H atom) (eV)	*N_2 (with H atom) (eV)
P–Ti@CN	-3.26	-3.11	-1.23	-1.14
P–V@CN	-3.26	-2.85	-1.12	-0.88
P–Cr@CN	-2.75	-2.34	-0.65	-0.50
P–Mn@CN	-2.70	-2.27	-0.74	-0.37
P–Co@CN	-2.69	-2.15	-1.01	-0.28
P–Ni@CN	-2.06	-1.77	-1.06	-0.10
P–Cu@CN	-1.20	-1.10	-0.41	-0.51

Table S8. The possible reaction pathways of NORR for electrochemical synthesis of NH_3.

O-distal	*NO → *NOH → *N → *NH → *NH_2 → *NH_3
O-alternating	*NO → *NOH → *HNOH → *NH → *NH_2 → *NH_3
N-distal	*NO → *HNO → *HNOH → *H_2NOH → *NH_2 → *NH_3
N-alternating	*NO → *HNO → *H_2NO → *H_2NOH → *NH_2 → *NH_3
Mixed-I	*NO → *NOH → *HNOH → *H_2NOH → *NH_2 → *NH_3
Mixed-II	*NO → *HNO → *HNOH → *NH → *NH_2 → *NH_3

**Table S9.** The adsorption energies of NO dimers for different adsorption configurations on P−Cu@CN, S−Ni@CN and S−Cu@CN.

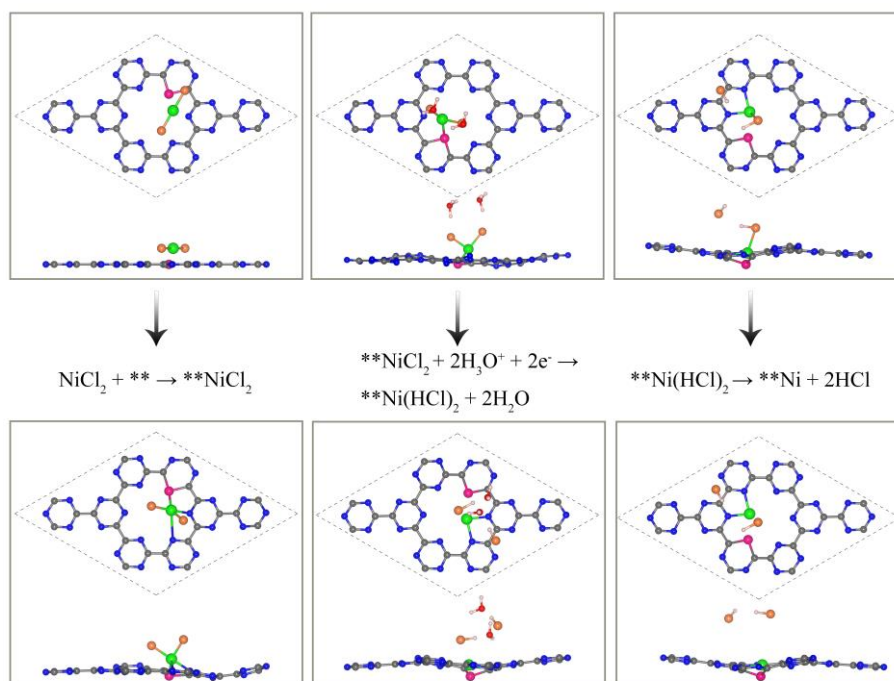|	*NNOO (eV)	*OONN (eV)	*ONNO (eV)
P-Cu@CN	-2.16	-1.98	-1.69
S−Ni@CN	-2.25	-1.01	
S−Cu@CN	-1.91	-2.05	
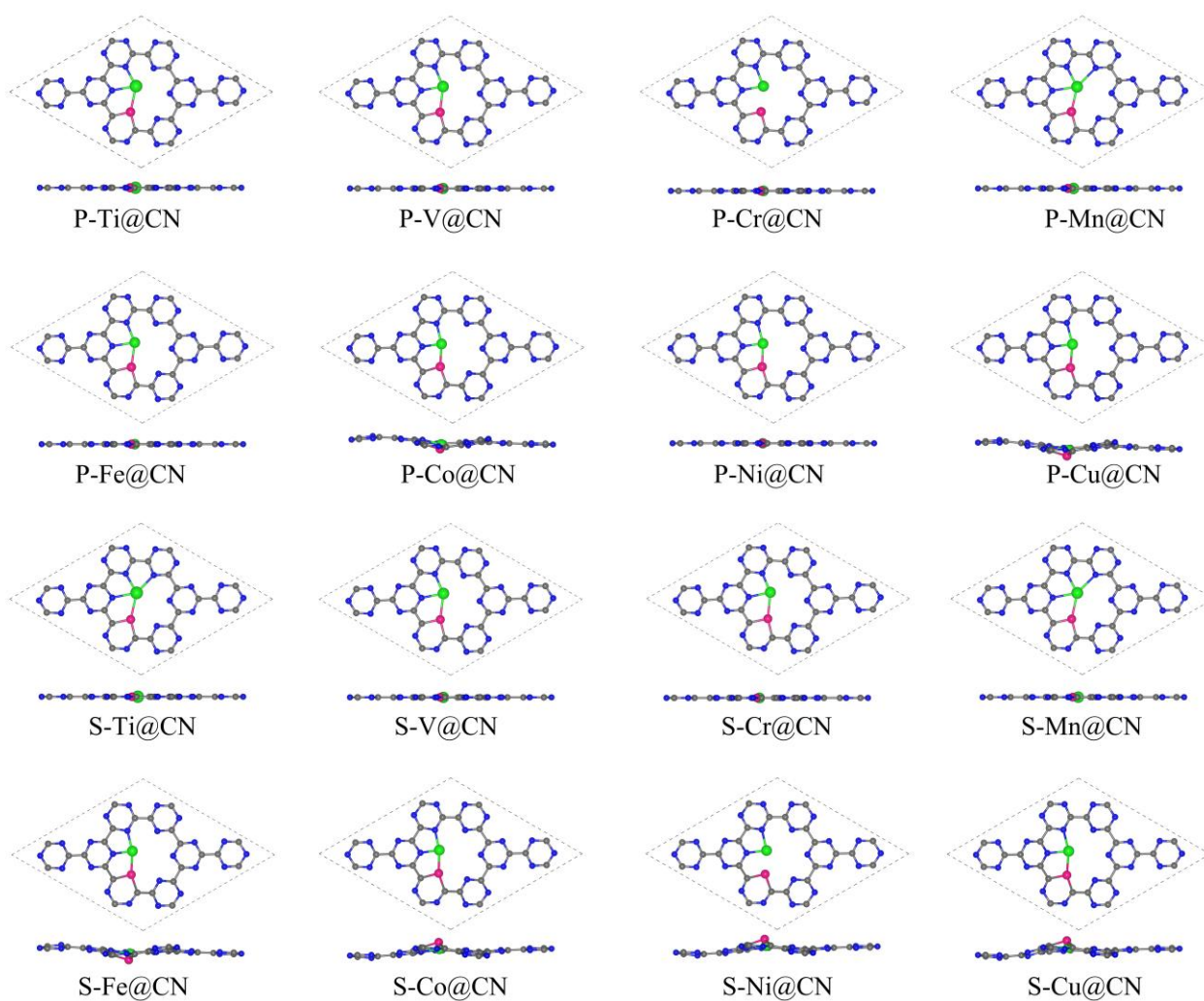
Fig. S1. Top and side views of the optimized Type1 configuration for P/S−TM@CN (TM= Ti, V, Cr, Mn, Fe, Co, Ni and Cu).
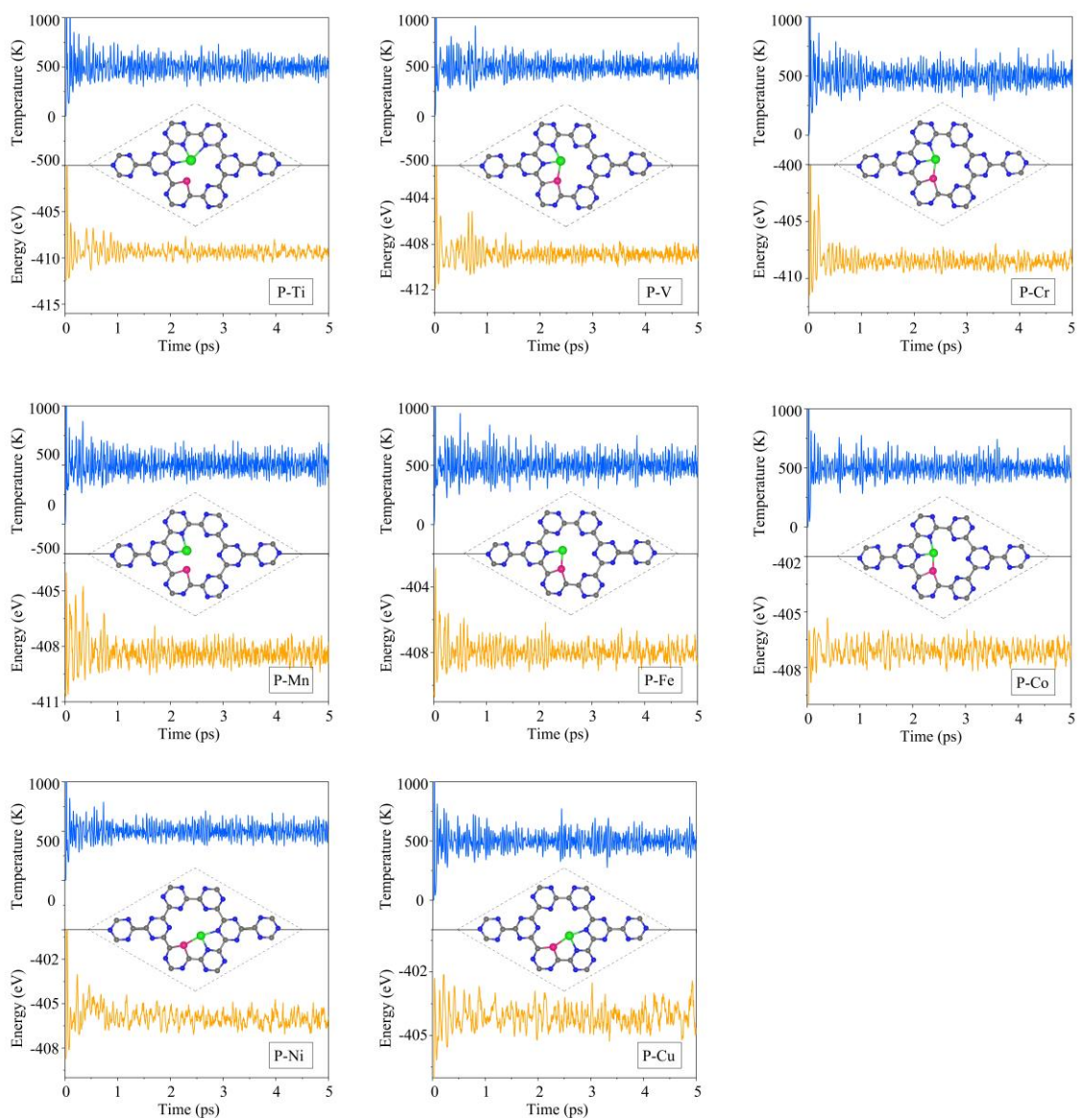
Fig. S2. The molecular dynamic (MD) simulation of P−TM@CN (TM = Ti, V, Cr, Mn, Fe, Co, Ni and Cu) at 500 K during 5 ps.
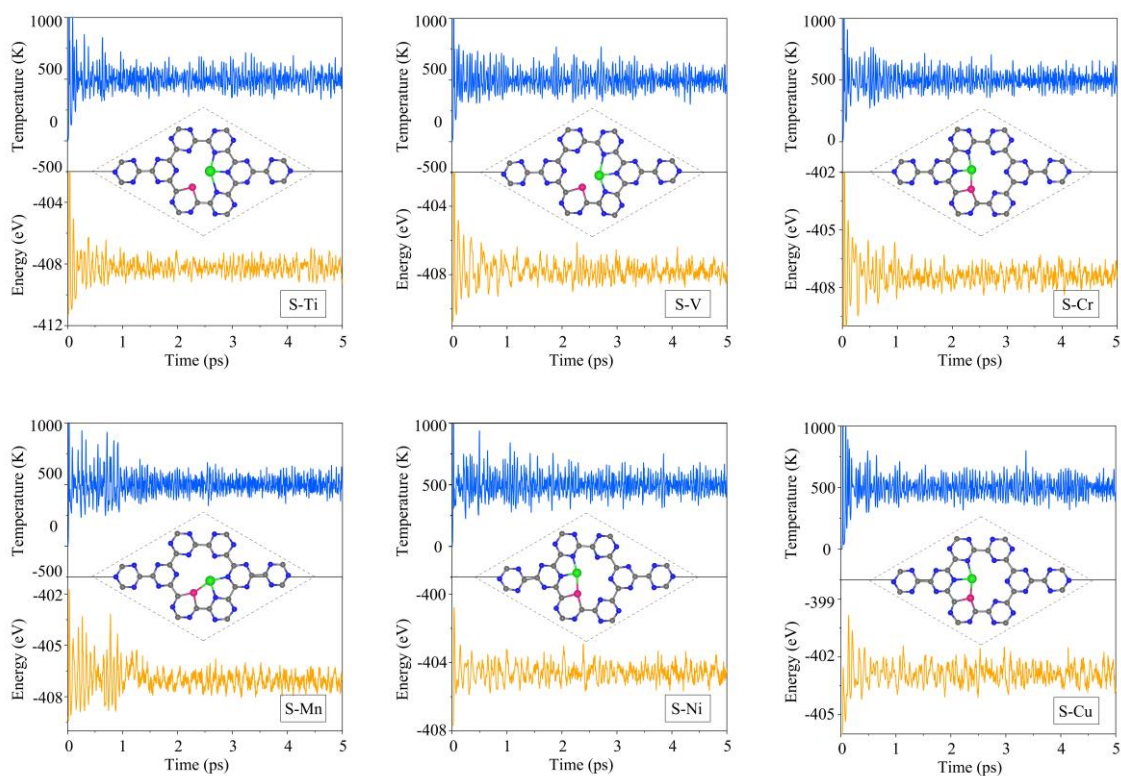
Fig. S3. The molecular dynamic (MD) simulation of S–TM@CN (TM = Ti, V, Cr, Mn, Ni and Cu) at 500 K during 5 ps.

$NiCl_2 + ** \rightarrow **NiCl_2$

$**NiCl_2 + 2H_3O^+ + 2e^- \rightarrow **Ni(HCl)_2 + 2H_2O$

$**Ni(HCl)_2 \rightarrow **Ni + 2HCl$

Fig. S4. The designed synthetic route for S-Ni@CN. Orange and red atoms represent Cl and O atoms, respectively.
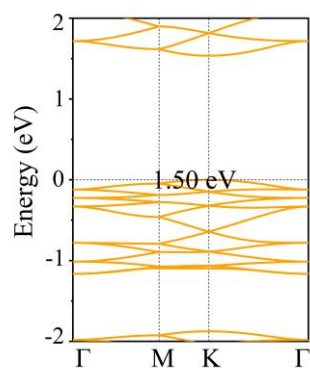
Fig. S5. Spin-polarized band structures of pristine CN. The Fermi level is set to 0 eV.
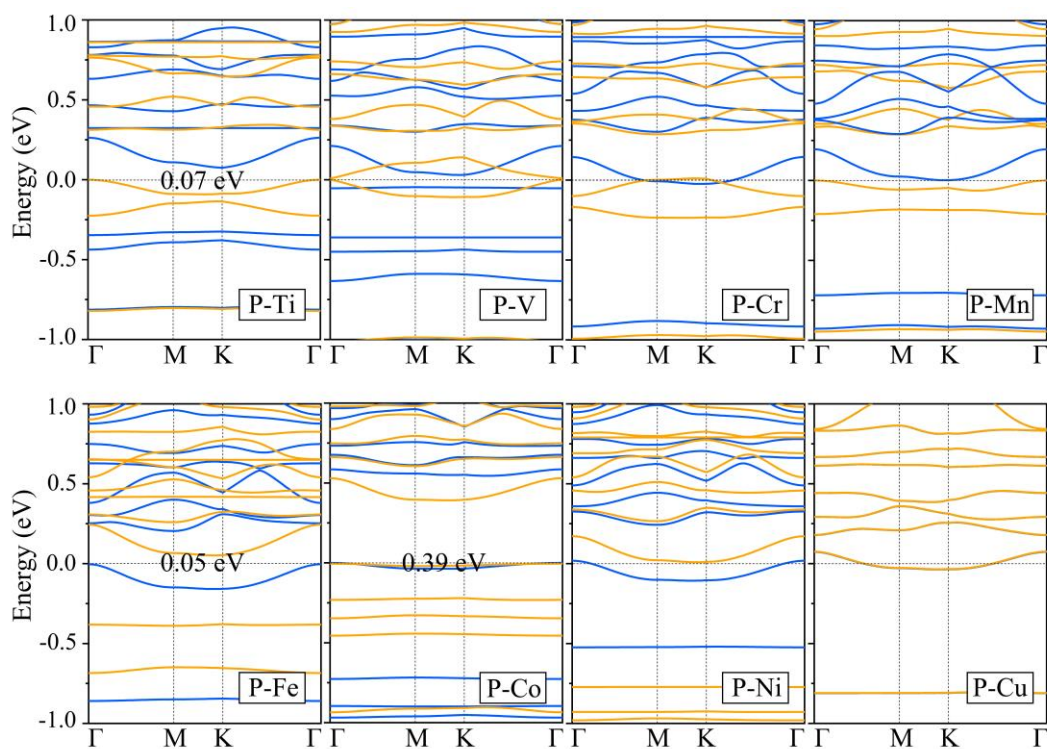
Fig. S6. Spin-polarized band structures of P–TM@CN. The blue and yellow lines represent spin-up and spin-down states, respectively. The Fermi level is set to 0 eV.
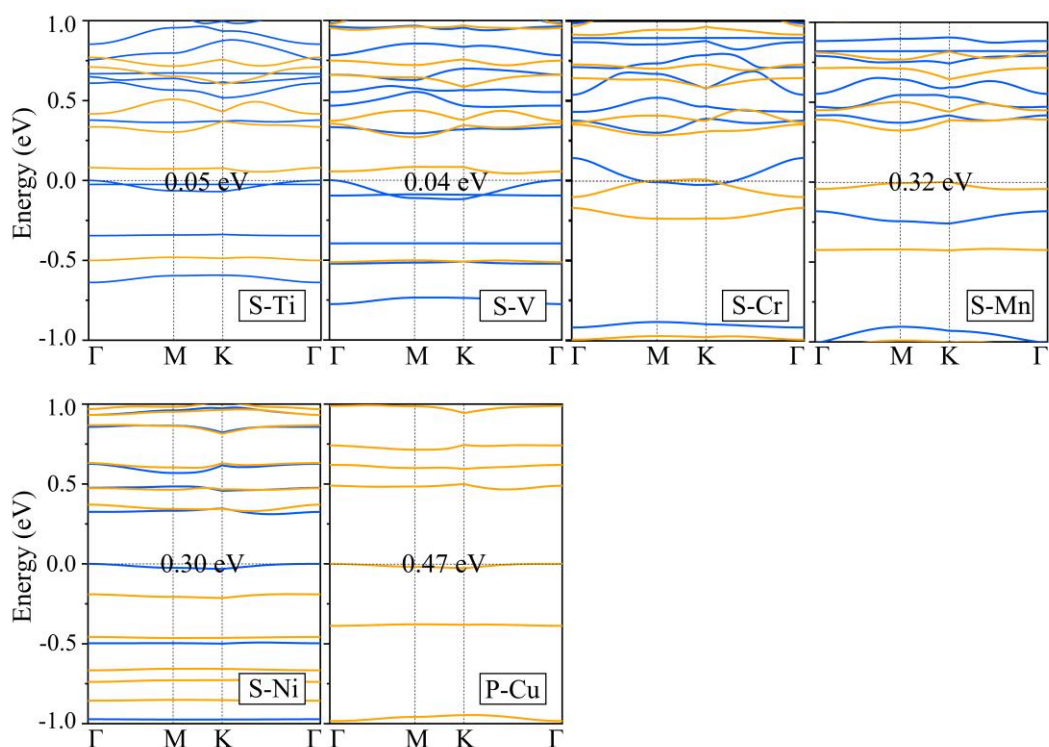
Fig. S7. Spin-polarized band structures of S–TM@CN. The blue and yellow lines represent spin-up and spin-down states, respectively. The Fermi level is set to 0 eV.
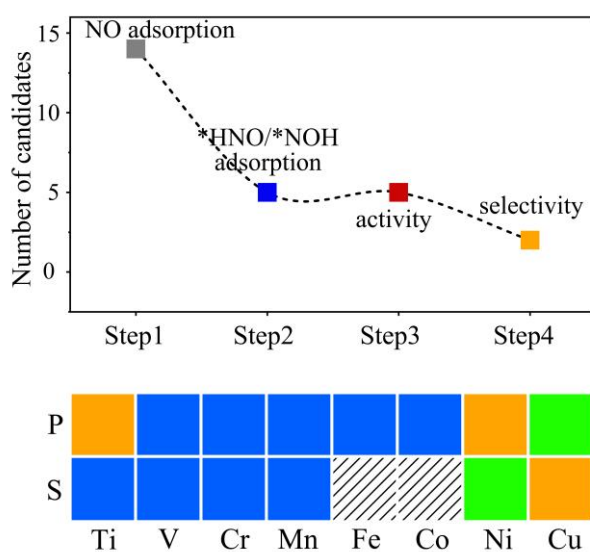
Fig. S8. Schematic illustration (top panel) of "four-step" strategy applied to screen NORR candidates, and the bottom panel is corresponding color codes map. The gray, blue, red and orange color codes represent the ruled out systems from each step, and the green color code represent the final selected candidates. In addition, the gray shadows indicate the non-existence of the corresponding candidates.
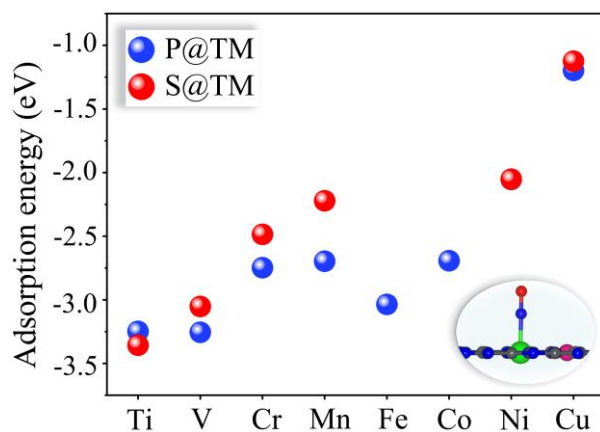
Fig. S9. Adsorption energies of NO on P/S−TM@CN (TM = Ti, V, Cr, Mn, Fe, Co, Ni and Cu) under the corresponding most stable adsorption configuration.
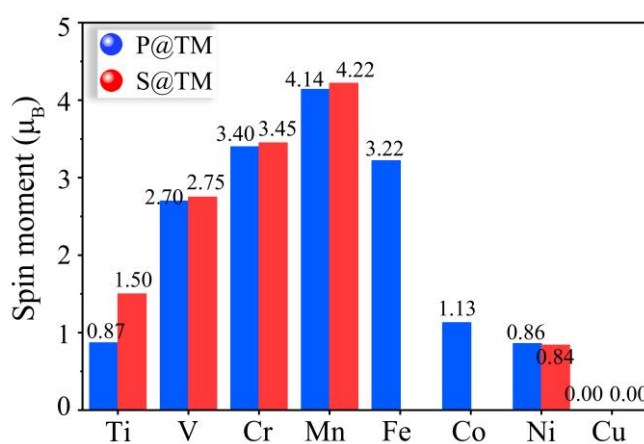
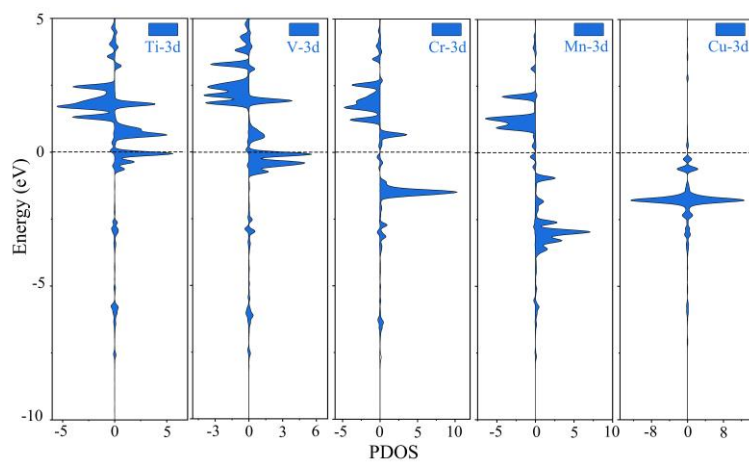**Fig. S10.** Spin magnetic moment on TM atom for P/S−TM@CN.
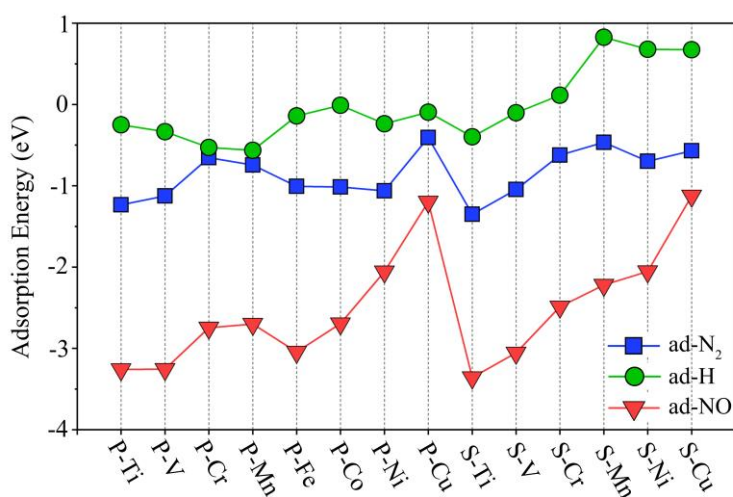
Fig. S11. The comparison of H proton, N_2 and NO adsorption energies on 14 P/S−TM@CN (TM = Ti, V, Cr, Mn, Fe, Co, Ni and Cu).
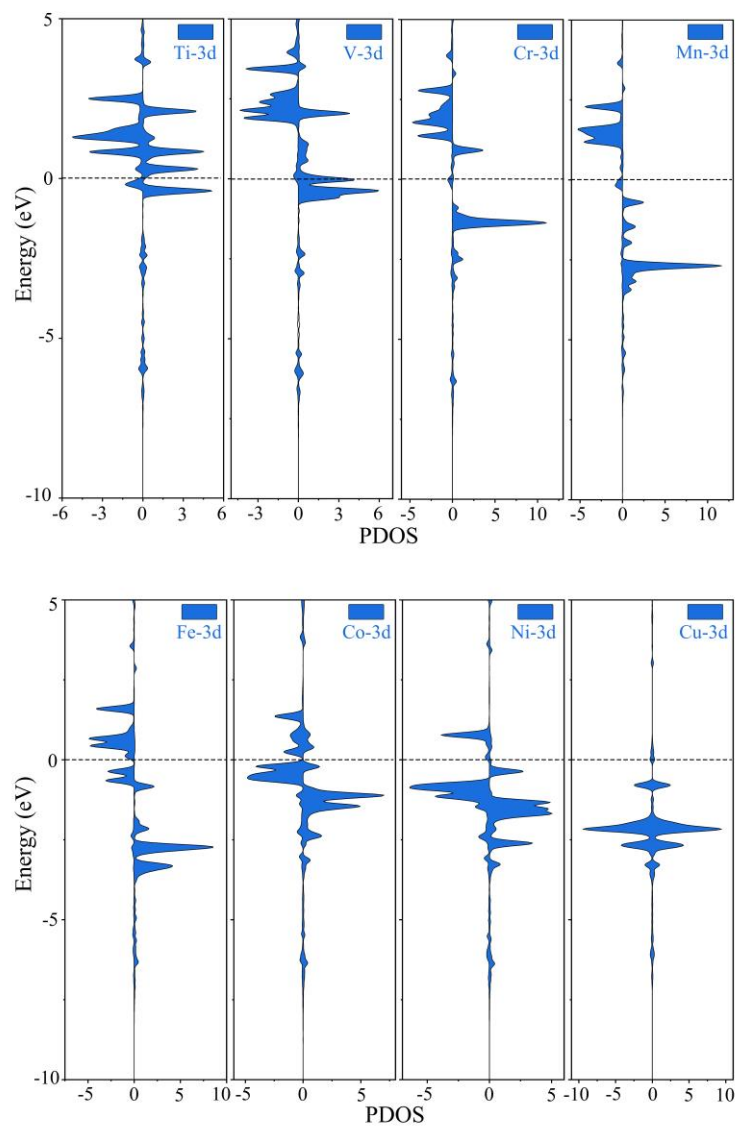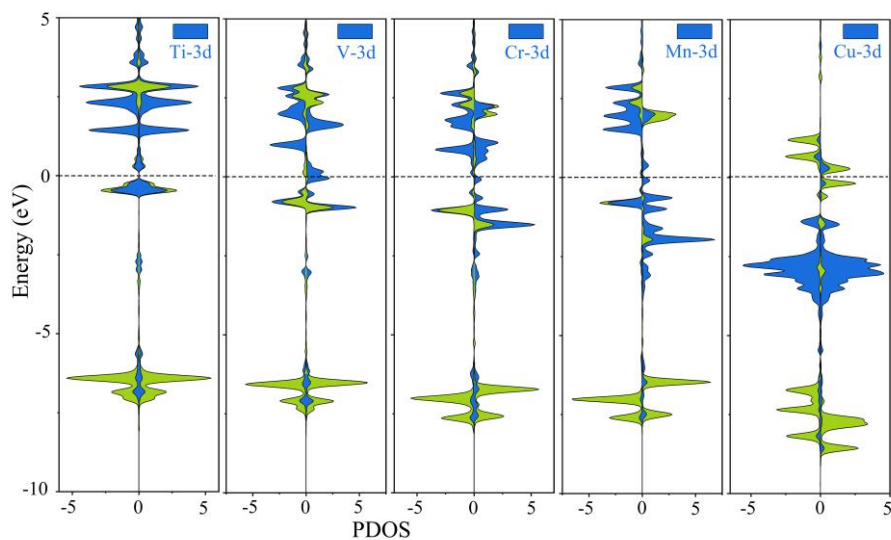
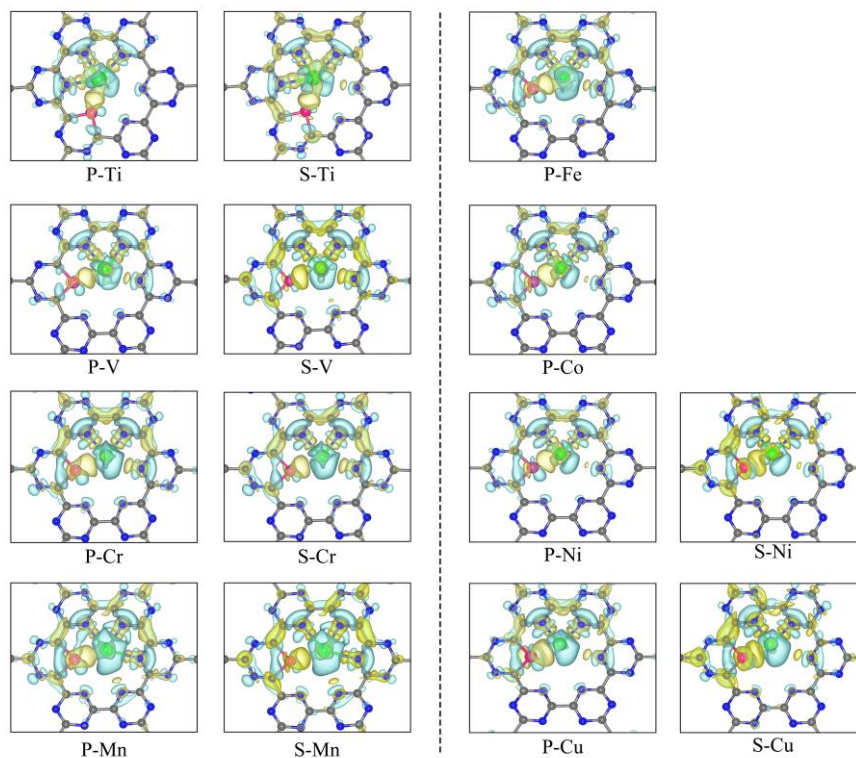**Fig. S12.** PDOS of P−TM@CN (TM = Ti, V, Cr, Mn, Fe, Co, Ni and Cu). The Fermi level is set to 0 eV.
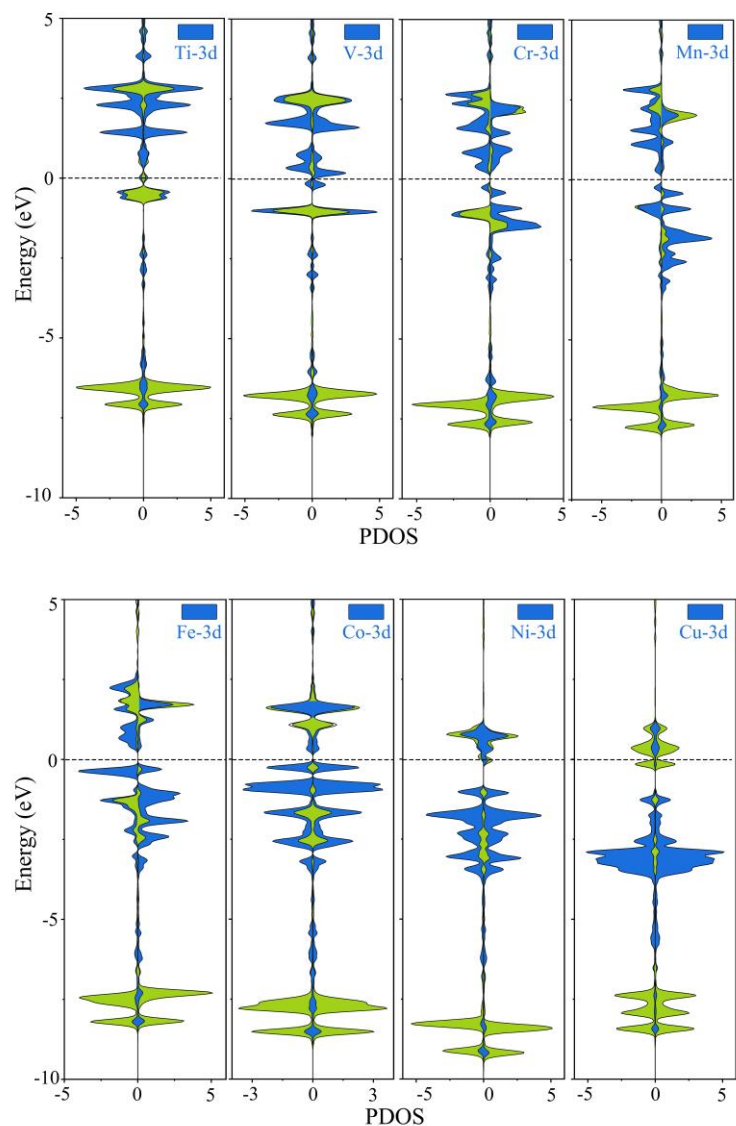
Fig. S13. PDOS of NO adsorbed P−TM@CN (TM = Ti, V, Cr, Mn, Fe, Co, Ni and Cu). The NO-2p orbitals are represented by green, and the Fermi level is set to 0 eV.


Fig. S14. PDOS of S−TM@CN (TM = Ti, V, Cr, Mn and Cu). The Fermi level is set to 0 eV.

Fig. S15. PDOS of NO adsorbed S–TM@CN (TM = Ti, V, Cr, Mn and Cu). The NO-2p orbitals are represented by green, and the Fermi level is set to 0 eV.


Fig. S16. Charge density differences of P/S–TM@CN (TM = Ti, V, Cr, Mn, Fe, Co, Ni and Cu) before NO adsorption, where the isosurface value is 0.004 e $Å^{-3}$ and yellow (blue) isosurface denote electron accumulation (depletion) areas.
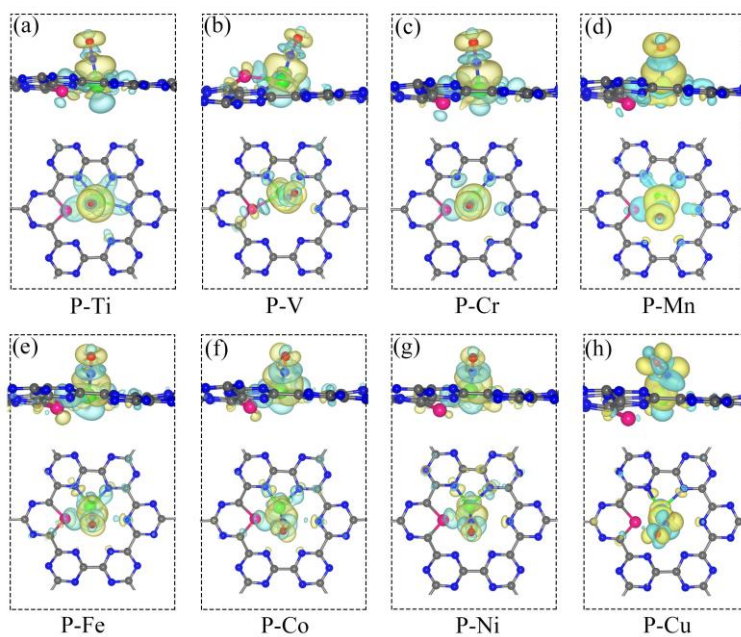
Fig. S17. Charge density differences of P–TM@CN (TM = Ti, V, Cr, Mn, Fe, Co, Ni and Cu) after NO adsorption, where the isosurface value is 0.004 e Å^{-3} and yellow (blue) isosurface denote electron accumulation (depletion) areas.
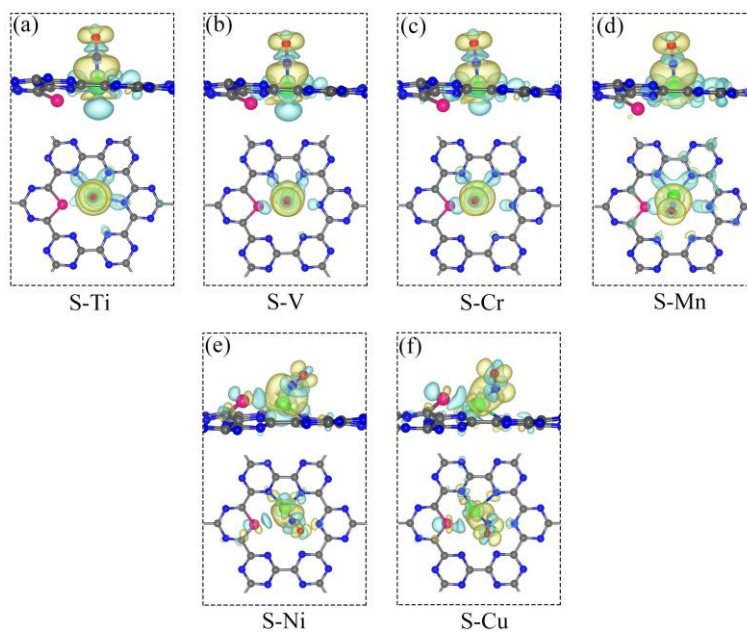
Fig. S18. Charge density differences of S–TM@CN (TM = Ti, V, Cr, Mn, Ni and Cu) after NO adsorption, where the isosurface value is 0.004 e Å^{-3} and yellow (blue) isosurface denote electron accumulation (depletion) areas.
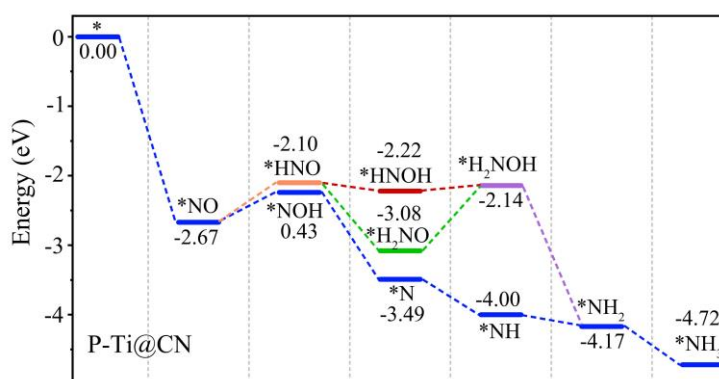
Fig. S19. Gibbs free energy diagram of NORR for electrochemical synthesis of NH$_3$ through different pathways on P−Ti@CN.
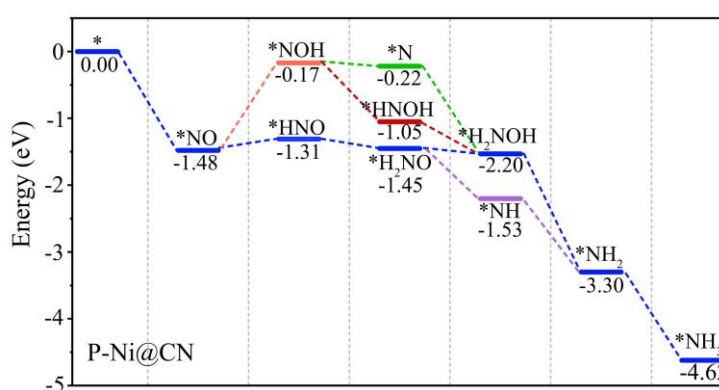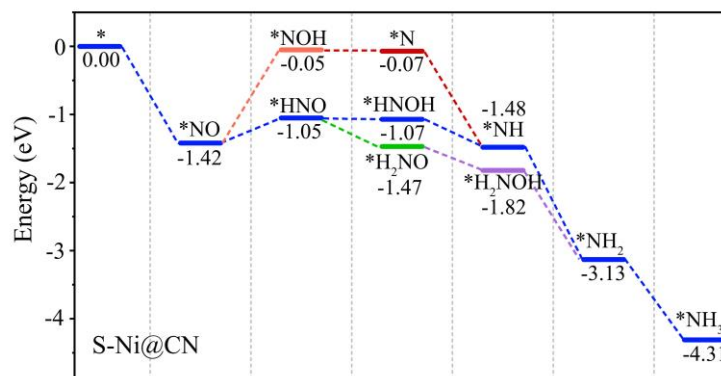

Fig. S20. Gibbs free energy diagram of NORR for electrochemical synthesis of NH$_3$ through different pathways on P−Ni@CN.
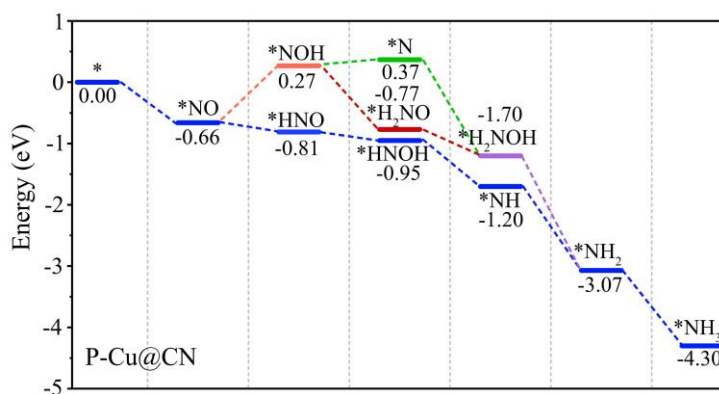
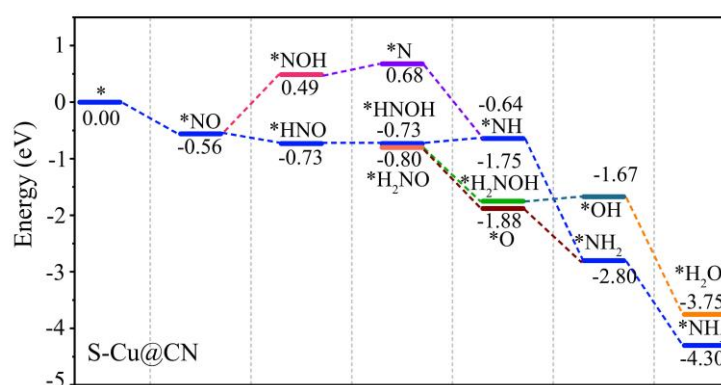**Fig. S21.** Gibbs free energy diagram of NORR for electrochemical synthesis of NH$_3$ through different pathways on P−Cu@CN.
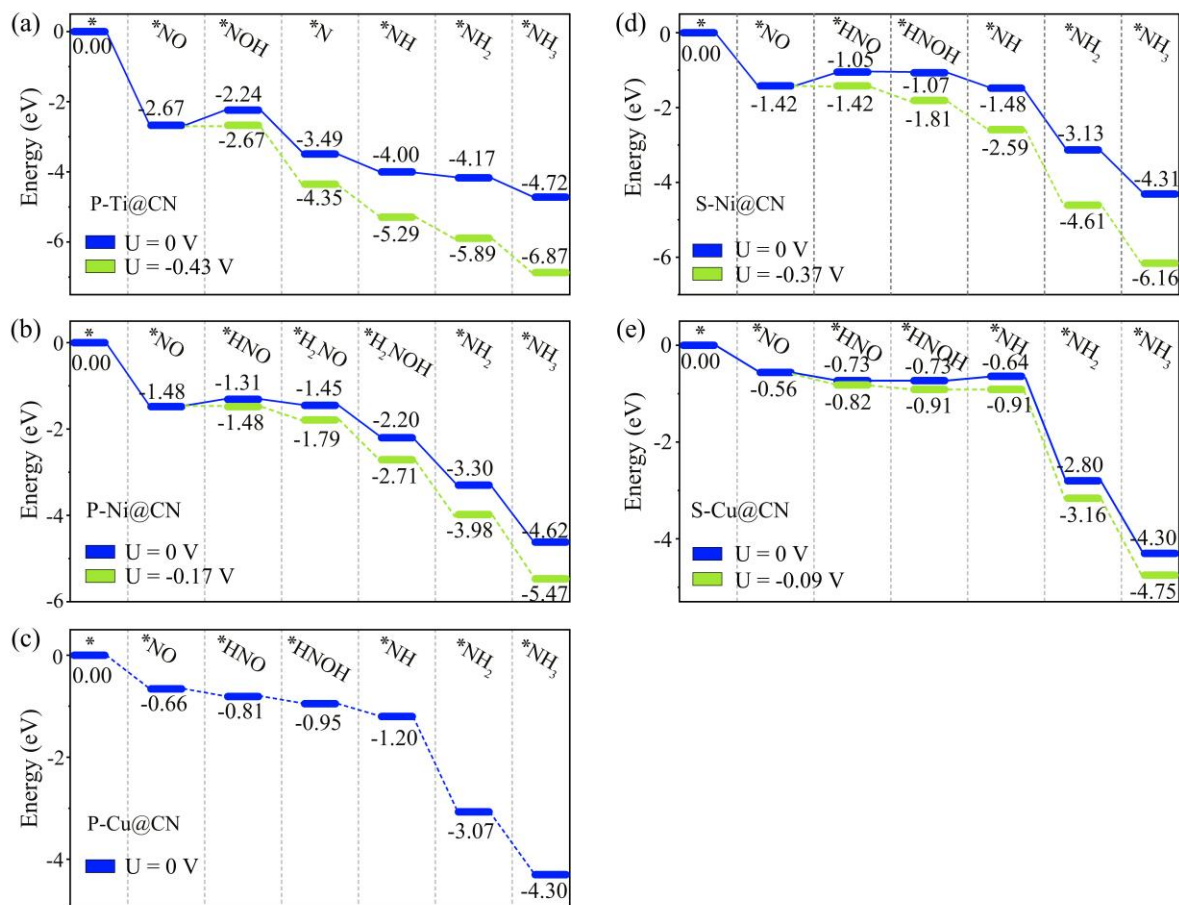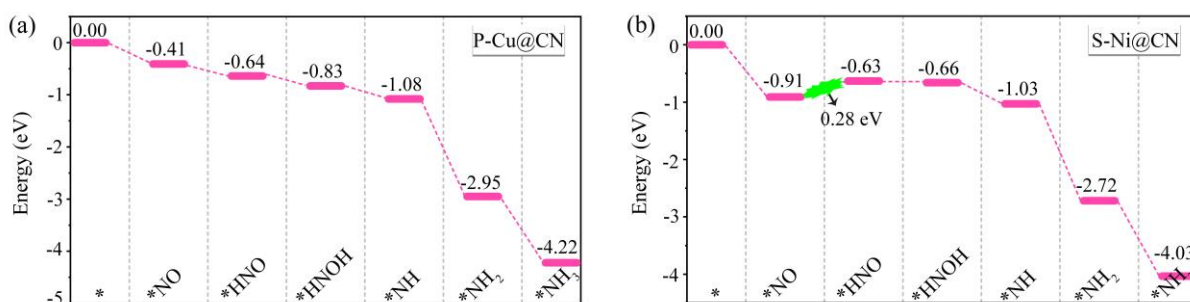
Fig. S22. Gibbs free energy diagram of NORR for electrochemical synthesis of NH$_3$ through different pathways on S−Ni@CN.
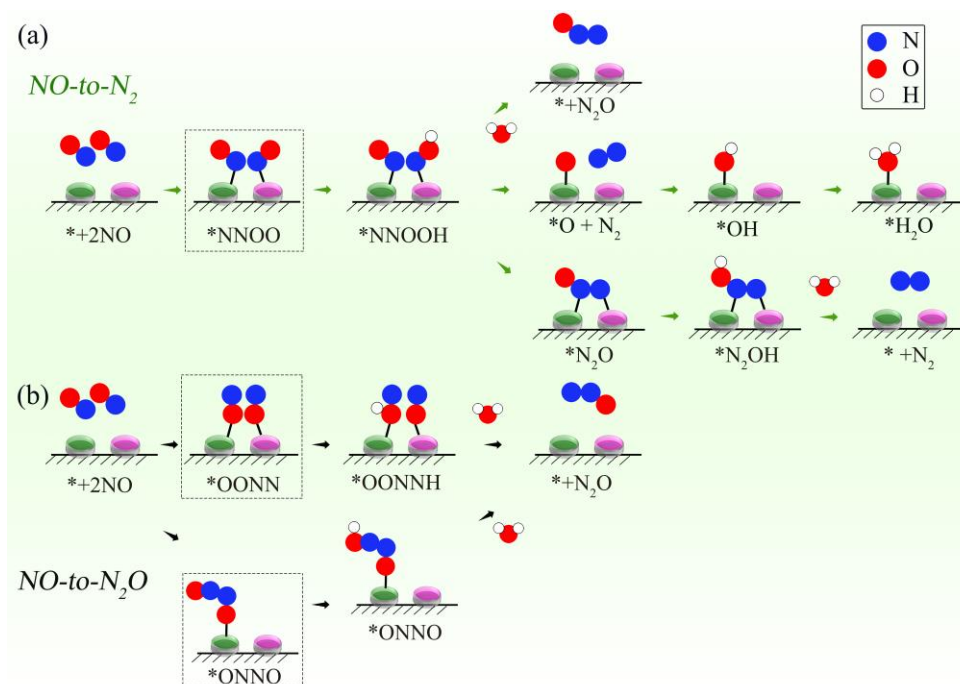

Fig. S23. Gibbs free energy diagram of NORR for electrochemical synthesis of NH$_3$ through different pathways on S−Cu@CN.
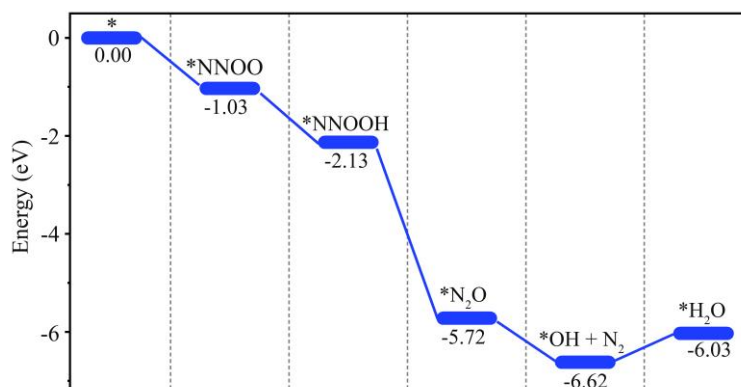
Fig. S24. Gibbs free energy diagrams of NORR for electrochemical synthesis of NH$_3$ at different applied potentials on (a) P–Ti@CN, (b) P–Ni@CN, (c) P–Cu@CN, (d) S–Ni@CN and (e) S–Cu@CN through their most favorable pathway, respectively.
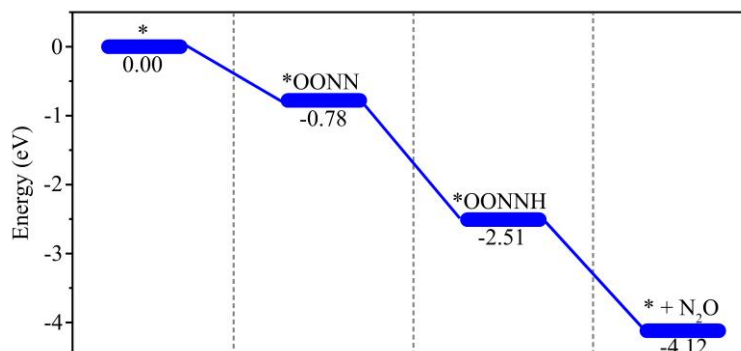

Fig. S25. Gibbs free energy diagrams of NORR for electrochemical synthesis of NH$_3$ on (a) P–Cu@CN and (b) S–Ni@CN in consideration of the Hubbard U correlation effect.

Fig. S26. Schematic illustration of the possible intermediates and reaction pathways of NORR for electrochemical synthesis of (a) N_2 and (b) N_2O, respectively.

Fig. S27. Gibbs free energy diagram of NORR for electrochemical synthesis of N_2 through the most favorable pathway on P−Cu@CN.

Fig. S28. Gibbs free energy diagram of NORR for electrochemical synthesis of N_2O through the most favorable pathway on S−Cu@CN.
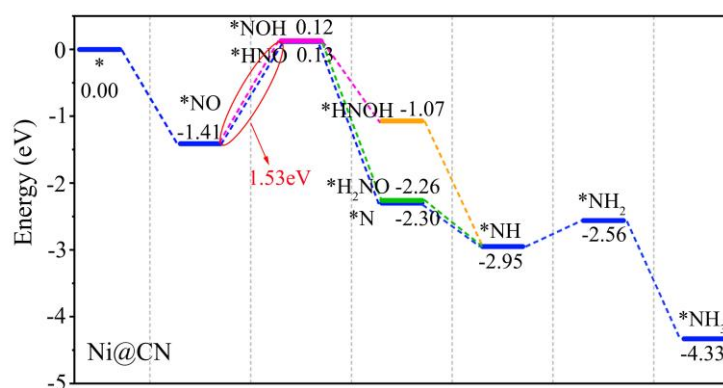
Fig. S29. Gibbs free energy diagram of NORR for electrochemical synthesis of NH$_3$ through different pathways on Ni@CN.

References

[1] L. Zhang, X. Jiang, Z. Zhong, L. Tian, Q. Sun, Y. Cui, X. Lu, J. Zou, S. Luo, *Angew. Chem. Int. Ed.* 2021, **60**, 21751–21755.

[2] S. Ajmal, A. Rasheed, N. Tran, X. Shao, J. Hwang, Y. Kim, J. Kim, H. Lee, *Appl. Catal. B: Environ.* 2023, **321**, 122070.

[3] S. Zhu, K. Wan, H. Wang, L. Guo, X. Shi, *Nanotechnology* 2021, **32**, 385404.

[4] S. Shinde, C. Lee, J. Yu, D. Kim, S. Lee, J. Lee, *ACS Nano* 2018, **12**, 596–608.

[5] M. He, W. An, Y. Wang, Y. Men, S. Liu, *Small*, 2021, **17**, 2104445.

[6] X. Lv, W. Wei, B. Huang, Y. Dai, T. Frauenheim, *Nano Lett.* 2021, **21**, 1871–1878.

[7] C. Ling, L. Shi, Y. Ouyang, X. Zeng, J. Wang, *Nano Lett.* 2017, **17**, 5133–5139.